Original Manuscript

Journal of Vibration and Control
2025, Vol. 0(0) 1–15

DOI: 10.1177/10775463251341758
journals.sagepub.com/home/jvc


Double tuned mass damper with a grounded inerter for structural vibration control

Huong Quoc Cao

Abstract

A Double Tuned Mass Damper (DTMD), which consists of a Tuned Mass Damper (TMD) connected in series with an undamped TMD, has been proven to be more efficient than a traditional TMD in previous studies. To enhance the vibration control performance and robustness of DTMD, an innovative type of DTMD for suppressing structural responses is proposed in this research. This new design includes a DTMD connected to the ground by a linear inerter (abbreviated as DTMDI). After establishing the analytical model of the DTMDI-structure system, the optimal configurations of the DTMDI for different values of inertance are obtained using the Balancing Composite Motion Optimization (BCMO). The effects of the variation in the structural properties as well as the weight and inertance of DTMDI on the performance and robustness of DTMDI are investigated. The present work indicates that an optimal DTMDI is much more effective and robust compared with an optimal DTMD with the same weight. Specifically, the DTMDI configuration with a higher inertance ratio demonstrates increased effectiveness. Moreover, the performance of the DTMDI surpasses that of a TMDI when both have the same mass and inertance, leading to a considerable reduction in the additional weight of the vibration absorber on the primary structure when using the DTMDI instead of the TMDI. While the DTMDI is more robust than both the DTMD and TMD against changes in the structure's natural frequency, it does not exhibit the same level of robustness as the TMDI when the natural frequency of the structure increases.

Keywords

Vibration control, double tuned mass damper inerter, tuned mass damper inerter, passive vibration absorber, multi-objective optimization

1. Introduction

Suppressing structural vibrations is a crucial requirement for civil structures under natural hazards (e.g., storms and earthquakes) to ensure comfort for occupants and structural safety (Balendra et al., 1995; Shah and Usman, 2022). Vibration control techniques and strategies have been investigated and successfully applied to worldwide civil structures (Bui et al., 2023a; Chang, 1999; Chang and Hsu, 1998; Di Matteo et al., 2022). One of these techniques is adding one or many vibration absorbers to the primary structure (Araz and Elias, 2024; Cao et al., 2024b; Gao et al., 1999; Pisal and Jangid, 2016; Samali et al., 2004; Tran et al., 2025; Wu et al., 2005). In this way, the most common damper type is TMD (including TLCD), because they are simple and effective dampers (Araz, 2021; Diana et al., 2013; Gao et al., 1999; Momtaz et al., 2017; Vellar et al., 2019; Yalla and Kareem, 2000).

TMDs have been utilized to suppress dynamic responses of structures under different types of loads (e.g., earthquakes, wind, or traffic loads). To enhance control performance of traditional TMDs, researchers have developed advanced types of TMDs (Araz, 2021a, 2024; Araz and Kahya, 2021; Hui et al., 2024; Kahya and Araz, 2019; Wang et al., 2022, 2024; Zuo, 2009). For example, Wang et al. (2024) suggested a novel tuned liquid mass damper for

School of Mechanical and Mechatronic Engineering, Faculty of Engineering and Information Technology, University of Technology Sydney, NSW, Australia

Corresponding author:
Huong Quoc Cao, School of Mechanical and Mechatronic Engineering, Faculty of Engineering and Information Technology, University of Technology Sydney, 15 Broadway, Ultimo NSW 2007, Australia.
Email: huong.q.cao@student.uts.edu.au

vertical vibration control of a large-span cable-stayed bridge in low-frequency domain, while Araz (2024) used multiple TMDs connected in parallel (MTMD) to reduce of structural vibrations. One of these innovative types of TMDs is inerter-based TMDs which show their noteworthy potential (Baduidana and Kenfack-Jiotsa, 2024; De Angelis et al., 2019; De Domenico and Ricciardi, 2018; Marian and Giaralis, 2014; Pandey and Mishra, 2021; Prakash and Jangid, 2022).

The concept of inerter was first suggested by Smith based on the force-current analogy between the electrical and mechanical networks (Smith, 2002). After that, Marian and Giaralis developed a tuned mass damper inerter to reduce the oscillatory motion of structural systems (Marian and Giaralis, 2014). Pandey and Mishra introduced the inerter-based compliant liquid column damper (TLCDI), proving its effectiveness in reducing dynamic responses for both single-degree-of-freedom (SDOF) and multi-degree-of-freedom (MDOF) structures under the recorded motions (Pandey and Mishra, 2021). Likewise, Wang et al. successfully employed a TLCDI to significantly mitigate the seismic response of SDOF structures (Wang et al., 2020). Moreover, Di Matteo et al. presented an innovative optimization procedure for designing TLCDIs, utilizing a statistical linearization technique that minimizes structural displacement differences, an essential factor for improving performance (Di Matteo et al., 2022). For dynamic vibration absorbers (DVAs), Baduidana and Kenfack-Jiotsa developed a three-element DVA with grounded stiffness and an attached inerter, designed specifically for controlling vibrations in undamped SDOF structures (Baduidana and Kenfack-Jiotsa, 2024). Additionally, Kendo-Nouja et al. proposed a grounded inerter-based DVA that efficiently reduces structural vibrations under both harmonic and random excitations (Kendo-Nouja et al., 2024). The outstanding results from these studies indicate that inerter-based vibration absorbers far outperform traditional ones, offering a robust solution for managing vibrations in various structural applications.

Cao and Tran (2023) introduced an innovative model of a DTMD. This device works as a passive control system intended to mitigate structural vibrations. The DTMD consists of a conventional TMD interconnected in series with a larger, undamped TMD. The worthy findings in their research work showed that the DTMD outperforms a conventional TMD with equivalent mass when it is used to reduce dynamic responses in structures. Building upon this foundational work, the present study proposes an upgraded version of the DTMD. This innovation version consists of a DTMD connected to the ground through a linear inerter (denoted as DTMDI). Obviously, DTMDI is not as simple as TMDI from the dynamics and structural viewpoints. However, based on how to connect a DTMDI and a TMDI with the main structure, the DTMDI is more straightforward than the TMDI because the DTMDI only needs a link point on the structure instead of two connection points as the TMDI.

In order to evaluate the structural vibration control performance of the proposed DTMDI absorber under harmonic excitations, a model of a DTMDI integrated into a SDOF structure under an external force is presented in Section 2. The optimal parameters of the DTMDI are then determined using a potential optimization algorithm in Section 3. Numerical simulations, results and discussions are presented in Section 4. Finally, the key conclusions of this work are shown in Section 5.

2. Analytical model of the DTMDI-structure system

An analytical model of a SDOF structure equipped with a DTMDI under an external force excitation is shown in Figure 1(a). This DTMDI consists of a DTMD linked to the ground through a linear inerter with an inertance value of b. It is important to note that the DTMD comprises two components, an undamped Tuned Mass Damper (referred to as TMD1) and a regular Tuned Mass Damper (referred to as TMD2), which are connected in series. The grounded inerter is linked to the DTMD at the TMD1. The reason why the author only uses the undamped TMD1 rather than a regular TMD1 was fully explained in Cao and Tran (2023). The mass and stiffness of TMD1 are M_1 and K_1, respectively, while the main parameters of TMD2 are the mass M_2 and the stiffness K_2 and the damping coefficient C_2. The key parameters of the primary structure include the generalized stiffness (K_s), the mass (M_s) and the damping coefficient (C_s). The external force acting on the primary structure, $F(t)$, in this work is assumed as a harmonic force excitation $F(t) = F_0 e^{j\omega t}$ with the excitation frequency ω and the force magnitude F_0.

There are many different types of inerters, in which three popular types are based on the inertial amplification mechanism including the rack and pinion type, ball and screw type, and hydraulic type inerters (Konar and Ghosh, 2024; Ma et al., 2021; Pandey and Mishra, 2021). Various inerter devices and their operating principles have been reported in previous works (Konar and Ghosh, 2024; Ma et al., 2021). A simplified model of a linear inerter is presented in Figure 1(b). As presented in the literature (Giaralis and Petrini, 2017; Pandey and Mishra, 2021; Wang et al., 2020), the inerter creates an inertia force $F_{AB} = b(\ddot{X}_B - \ddot{X}_A)$ between two terminals (A and B). For this study, the inertia force generated by the grounded inerter is $F_{inerter} = b(\ddot{X}_s + \ddot{X}_1)$, where

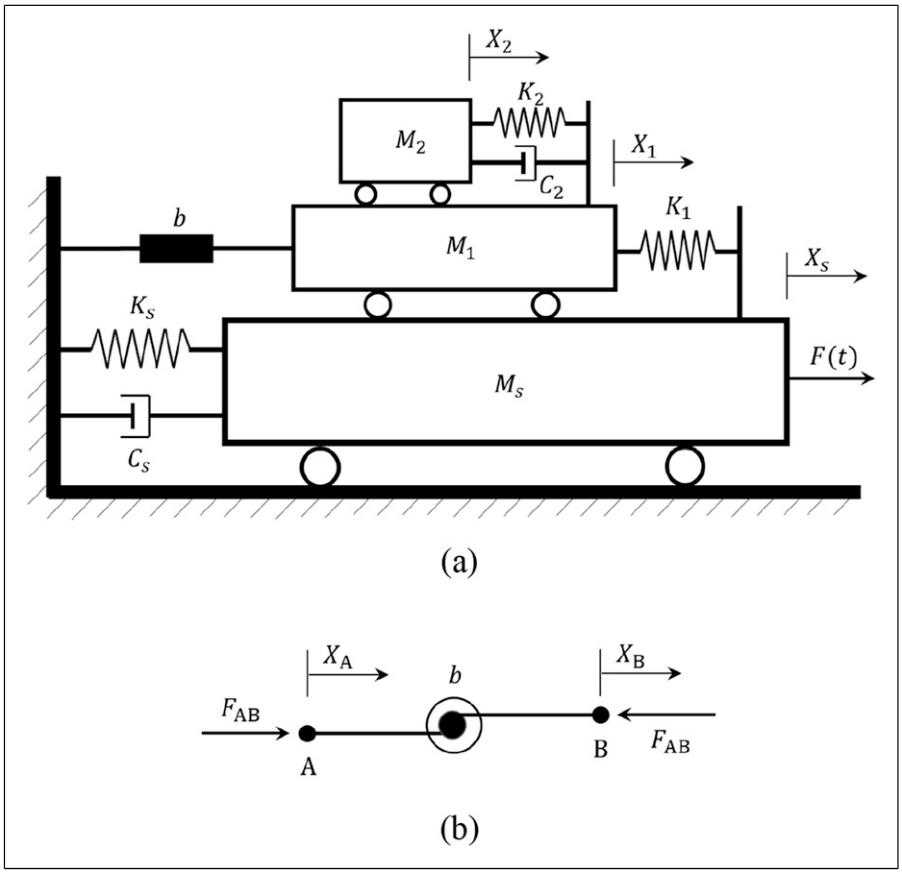

Figure 1. (a) Analytical model of the DTMDI-structure system. (b) Simplified model of a linear inerter.

$(\ddot{X}_s + \ddot{X}_1)$ is the acceleration of the mass M_1 relative to the ground.

The equations of motion of the system are given by

$$M_s\ddot{X}_s(t) + C_s\dot{X}_s(t) + K_sX_s(t) - K_1X_1(t) = F(t), \quad (1)$$

$$\begin{aligned}(M_1 + b)\ddot{X}_s(t) + (M_1 + b)\ddot{X}_1(t) \\ + K_1X_1(t) - C_2\dot{X}_2(t) - K_2X_2(t) = 0,\end{aligned} \quad (2)$$

$$M_2\left(\ddot{X}_s(t) + \ddot{X}_1(t) + \ddot{X}_2(t)\right) + C_2\dot{X}_2(t) + K_2X_2(t) = 0. \quad (3)$$

In the above equations, $X_s(t)$ denotes the horizontal displacement of the structure relative to the ground, $X_1(t)$ represents the horizontal motion of the TMD1 relative to the structure, and $X_2(t)$ is the horizontal displacement of the TMD2 relative to the TMD1. Therefore, the displacement of the mass M_1 relative to the ground is $X_s(t) + X_1(t)$. As previously mentioned, the inertia force generated by the grounded inerter is $F_{inerter} = b(\ddot{X}_s(t) + \ddot{X}_1(t))$, which is added to the TMD1 of the DTMD. This means that the total mass of the DTMDI (including its real mass and an apparent mass due to the grounded inerter) increased by b compared with that in the DTMD. Now, we introduce the following quantities.

The natural frequency of the primary structure

$$\omega_s = \sqrt{\frac{K_s}{M_s}}. \quad (4)$$

The damping ratio of the primary structure

$$\xi_s = \frac{C_s}{2M_s\omega_s}. \quad (5)$$

The natural frequency of the TMD1 in the DTMDI is

$$\omega_1 = \sqrt{\frac{K_1}{M_1 + b}}. \quad (6)$$

The natural frequency of the TMD2 in the DTMDI is

$$\omega_2 = \sqrt{\frac{K_2}{M_2}}. \quad (7)$$

The damping ratio of the TMD2 in the DTMDI is

$$\xi_2 = \frac{C_2}{2M_2\omega_2}. \tag{8}$$

The mass ratio of the TMD1 is

$$\mu_1 = \frac{M_1}{M_s}. \tag{9a}$$

and the mass ratio of the TMD2 is

$$\mu_2 = \frac{M_2}{M_s}. \tag{9b}$$

Therefore, the mass ratio between the DTMD and the structure is

$$\mu = \frac{M_1 + M_2}{M_s} = \mu_1 + \mu_2. \tag{9c}$$

Note that the mass ratio between the TMD2 and the TMD1 in the DTMDI is

$$\mu_{21} = \frac{\mu_2}{\mu_1} = \frac{M_2}{M_1}. \tag{9d}$$

The inertance ratio of the inerter is defined as

$$\eta = \frac{b}{M_s}. \tag{9e}$$

Hence, the total mass ratio between the DTMDI and the structure is determined by

$$\mu^* = \frac{M_1 + b + m_2}{M_s} = \mu + \eta, \tag{9f}$$

in which η is an imaginary mass added to the DTMD due to the grounded inerter. This leads to an increase in the mass of DTMD by $\eta = \frac{b}{M_s}$ compared with μ in DTMD.

As a result, equations (1)–(3) are rewritten in the matrix form as follows:

$$\mathbf{M}\ddot{\mathbf{X}} + \mathbf{C}\dot{\mathbf{X}} + \mathbf{K}\mathbf{X} = \mathbf{F}, \tag{10}$$

in which

$$\mathbf{M} = \begin{bmatrix} 1 & 0 & 0 \\ M_1 + b & M_1 + b & 0 \\ M_2 & M_2 & M_2 \end{bmatrix}, \tag{10a}$$

$$\mathbf{C} = \begin{bmatrix} 2\xi_s\omega_s & 0 & 0 \\ 0 & 0 & -2\mu_{21}\xi_2\omega_2 \\ 0 & 0 & 2\xi_2\omega_2 \end{bmatrix}, \tag{10b}$$

$$\mathbf{K} = \begin{bmatrix} \omega_s^2 & -\mu_1\omega_1^2 & 0 \\ 0 & \omega_1^2 & -\mu_{21}\omega_2^2 \\ 0 & 0 & \omega_2^2 \end{bmatrix}, \tag{10c}$$

Table 1. Key parameters of the main structure (Cao, 2023; Varadarajan and Nagarajaiah, 2004; Yang et al., 2004).

Parameter	Symbol	Value
The total mass	M_s	153e^6 kg
The natural frequency	ω_s	1.0 rad/s
The damping ratio	ξ_s	1%

$$\mathbf{F} = \begin{bmatrix} (F_0/M_0)e^{j\omega t} \\ 0 \\ 0 \end{bmatrix}, \tag{10d}$$

$$\mathbf{X} = \begin{bmatrix} X_s(t) \\ X_1(t) \\ X_2(t) \end{bmatrix}; \dot{\mathbf{X}} = \begin{bmatrix} \dot{X}_s(t) \\ \dot{X}_1(t) \\ \dot{X}_2(t) \end{bmatrix}; \ddot{\mathbf{X}} = \begin{bmatrix} \ddot{X}_s(t) \\ \ddot{X}_1(t) \\ \ddot{X}_2(t) \end{bmatrix}. \tag{10e}$$

The dynamic magnification factor (DMF) of the structural response in the steady state is given by (Den Hartog, 1985; Gil-Martín et al., 2012)

$$DMF = \frac{max X_s(t)}{(F_0/K_s)}. \tag{11}$$

Now, non-dimensional quantities are introduced as follows:

The frequency ratio is

$$\alpha = \frac{\omega}{\omega_s}. \tag{12}$$

The tuning ratio for the TMD1 of the DTMDI is

$$\beta_1 = \frac{\omega_1}{\omega_s} \tag{13a}$$

and the tuning ratio for the TMD2 of the DTMDI is

$$\beta_2 = \frac{\omega_2}{\omega_s}. \tag{13b}$$

The peak dynamic magnification factor of the structural response (DMF_{max}) in the frequency range which corresponds to $[\alpha_{lo}, \alpha_{up}]$ can be expressed by:

$$DMF_{max} = \frac{max\left(X_s(t)|_{\alpha_{lo}}^{\alpha_{up}}\right)}{(F_0/K_s)}. \tag{14}$$

In the above equation, α_{lo} and α_{up} are the lower and upper limits of the frequency ratio, respectively.

As a result, the structural frequency response is a function of $\alpha, \beta_1, \beta_2, \xi_s, \xi_2, b, \mu_1$ and μ_2. It is noted that ξ_s and α are determined from the key parameters of the structure and μ_1 and μ_2 can be calculated through μ and μ_{21}.

Table 2. The lower and upper limits of the parameters of DTMDI.

Parameter (Symbol)	Value
The mass ratio (μ_{21})	0.05< μ_{21} <5.0
The tuning ratio of the TMD1 (β_1)	0.5< β_1 <1.5
The tuning ratio of the TMD2 (β_2)	0.5< β_2 <1.5
The damping ratio of the TMD2 (ξ_2)	0 < ζ <0.5

To facilitate comparisons, the TMDI-structure system is also built, and its equations of motion are presented in Appendix A.

3. Parametric optimization

3.1. Input parameters

In the numerical examples presented in this work, the SDOF structure represents the first mode of a 76-story building, as used in the previous studies (Cao, 2023; Varadarajan and Nagarajaiah, 2004; Yang et al., 2004). The key parameters of this mode are detailed in Table 1. The excitation frequency ratio range is assumed to be between 0.5 and 1.5 ($0.5 \le \alpha \le 1.5$) and the external force magnitude is $F_0 = 7.5e^5$ N.

In this work, the mass ratio (μ) is fixed to be 0.02 for all cases considered. The inertance ratios including $\eta = 0\%$, 1%, 2%, 3%, 4%, and 5% are considered here. It is noted that when $\eta = 0\%$ (meaning $b = 0$), the DTMDI becomes the DTMD and the DTMDI-structure system will be the DTMD-structure system. In this study, the DTMD-structure system will also be used for the purpose of extensive comparisons in Section 4. Table 2 reports the lower and upper limits of the parameters that need to be optimized for a DTMDI.

3.2. Optimal parameters

The aim of the parametric optimization is to maximize the vibration control capacity of DTMDI. This means that the DMF_{max} value of the structural response as the excitation frequency changes in the domain of $[\omega_{\text{lo}}, \omega_{\text{up}}]$ corresponding to the frequency ratio range within $[\alpha_{\text{lo}}, \alpha_{\text{up}}]$ should be minimized. Thus, the objective function based on the *DMFmax* value is expressed by

$$Objective = min\left(DMF_{max}|_{\omega_{lo}}^{\omega_{up}}\right). \quad (15)$$

It is evident that the objective function, as shown in equation (15), has many variables and constraints. Hence, we need a potential optimization algorithm to solve this problem.

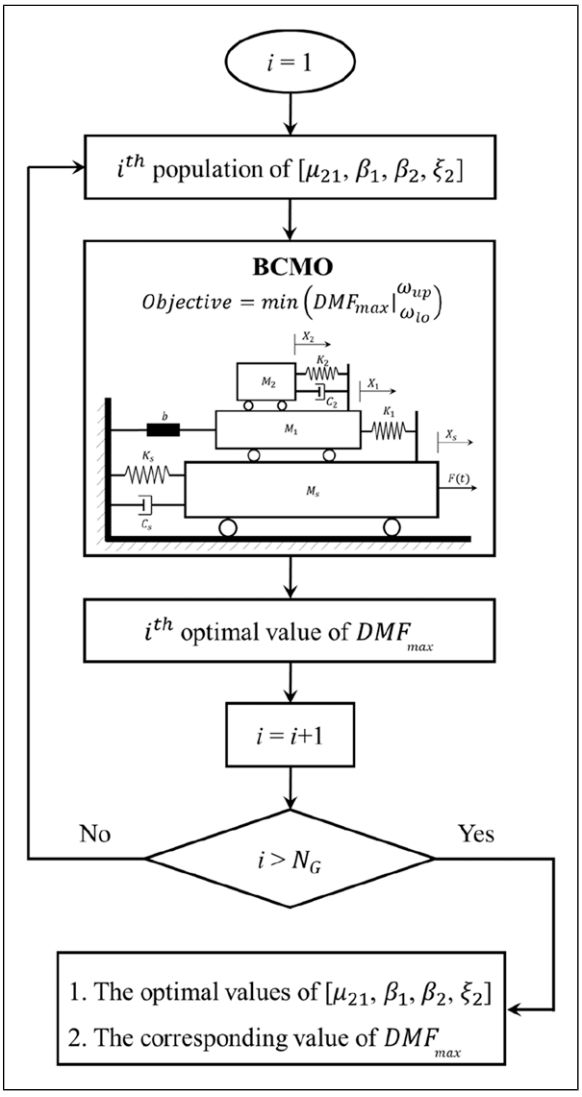

Figure 2. Diagram of the optimization procedure for the DTMDI using the BCMO algorithm.

There are many algorithms used to search solutions of optimization problems (Etedali and Rakhshani, 2018; Le-Duc et al., 2020; McCall, 2005), and one can use one of the existing techniques (e.g., Genetic Algorithms, Cuckoo Search Algorithm, Firefly Algorithm, and Moth-Flame Optimization) to optimize the DTMDI. Among the recently developed optimization algorithms, Balancing Composite Motion Optimization (BCMO) is a novel technique introduced by Le-Duc et al. (2020). Basically, the BCMO is a population-based optimization algorithm. The fundamental concept of this algorithm revolves around balancing the composite motion characteristics of individuals within the solution space. By integrating a probabilistic selection model, balancing global and local searches establishes a movement mechanism for each individual. The basic

Table 3. Optimal configurations of the DTMD and DTMDI with the different values of η.

	Fixed parameters		Optimal parameters of DTMD and DTMDI			
Device	η	μ	μ_{21}	β_1	β_2	ξ_2
DTMD	0%	2%	0.052	1.015	0.966	0.158
DTMDI	1%	2%	0.125	1.025	0.950	0.198
DTMDI	2%	2%	0.225	1.030	0.936	0.216
DTMDI	3%	2%	0.414	1.041	0.920	0.249
DTMDI	4%	2%	0.673	1.047	0.907	0.264
DTMDI	5%	2%	1.094	1.051	0.895	0.275

principles of the BCMO method were fully explained, and readers can find them in Ref. (Le-Duc et al., 2020) where the authors provided publicly available MATLAB source codes for this algorithm. The BCMO has demonstrated high efficiency, low complexity, and rapid convergence when compared with different population-based optimization algorithms. One can find those comparisons in the original work of Le-Duc et al. (2020). Additionally, the BCMO is also effective for multi-objective or complex optimization problems involving many variables and constraints (Bui et al., 2023; Le-Duc et al., 2020; Tran et al., 2024). Therefore, the BCMO is chosen to find the optimal parameters for absorbers in this research.

The BCMO algorithm has two main parameters, including the number of generations (N_G) and the number of individuals in the population (N_P). These parameters are selected depending on the number of variables and the convergence of the objective function. A flowchart of the design optimization procedure for the DTMDI is presented in Figure 2, in which the proposed device has four parameters (design variables) that need to be optimized. These design variables and their bounds are mentioned in Table 2.

Using the input parameters discussed in Section 3.1, Table 3 presents the optimized configurations for the DTMDI based on various values of η. These values include $\eta = 0\%$ for the DTMD and $\eta = 1\%$, 2%, 3%, 4%, and 5% for the DTMDI. For comparisons, Table 4 also includes the optimal TMDI configurations for the different η values (0%, 1%, 2%, 3%, 4%, and 5%) with $\mu = 2\%$. It is evident from both Table 3 and Table 4 that the optimal parameters for the TMD and DTMD at $\mu = 2\%$ are consistent with those reported in Refs (Cao, 2023; Cao and Tran, 2023). Additionally, based on the number of design variables and the convergence of the objective function in this study, two key parameters of the BCMO, N_G and N_P, are chosen to be 200 and 300, respectively.

The data presented in Table 3 offers valuable insights regarding the behavior of various design variables in relation to the importance ratio (η). Specifically, it indicates that as the inertance ratio increases, three key design variables (μ_{21}, β_1, and ξ_2) also increase. This is a direct correlation between the inertance ratio and these variables, which could be critical for optimizing performance. Conversely, the tuning ratio β_2 consistently declines as η increases from 1% to 5%. Variations in the DTMDI parameters associated with changes in the inertance ratio are illustrated in Figure 3, highlighting how a value of η significantly impact the tuning design variables.

Furthermore, the analysis suggests that achieving an optimal configuration for the DTMDI, particularly as the value of η rises, necessitates a larger damping ratio. It also indicates that an increase in μ_{21} is essential for maintaining stability and performance in such configurations. These findings emphasize the complexity of the design process and the importance of considering multiple interrelated factors when optimizing the DTMDI-structure system.

4. Numerical investigations and discussions

In this section, the author focuses on the effectiveness and robustness of the optimal DTMDI configurations, where effects of structural natural frequency on the vibration control performance of DTMDI and effects of the inerter on the structure response are considered.

4.1. Evaluation criteria

In this study, there are two primary criteria to evaluate the effectiveness of the DTMDI in controlling structural vibrations. The first criterion is DMF_{max}. This is a key indicator, and a device is deemed more effective in mitigating vibrations when it gives a lower DMF_{max} value (Yamaguchi and Harnpornchai, 1993). This factor reflects how much the vibrations are reduced in the controlled structure compared to the uncontrolled structure. The second criterion is the root mean square of the peak displacement response, denoted as RMS_X. A lower RMS_X value signifies that the device can dissipate more vibrational energy (Wu et al., 2018). While the peak dynamic magnification factor of the structural response is calculated using equation (14), the second criterion is given by (Wu et al., 2018).

Table 4. Optimal configurations of the TMD and TMDI with the different values of η.

	Fixed parameters		Optimal parameters of TMD and TMDI	
Device	η	μ	β	ξ
TMD	0%	2%	0.978	0.088
TMDI	1%	2%	0.968	0.129
TMDI	2%	2%	0.959	0.173
TMDI	3%	2%	0.949	0.215
TMDI	4%	2%	0.940	0.254
TMDI	5%	2%	0.931	0.297

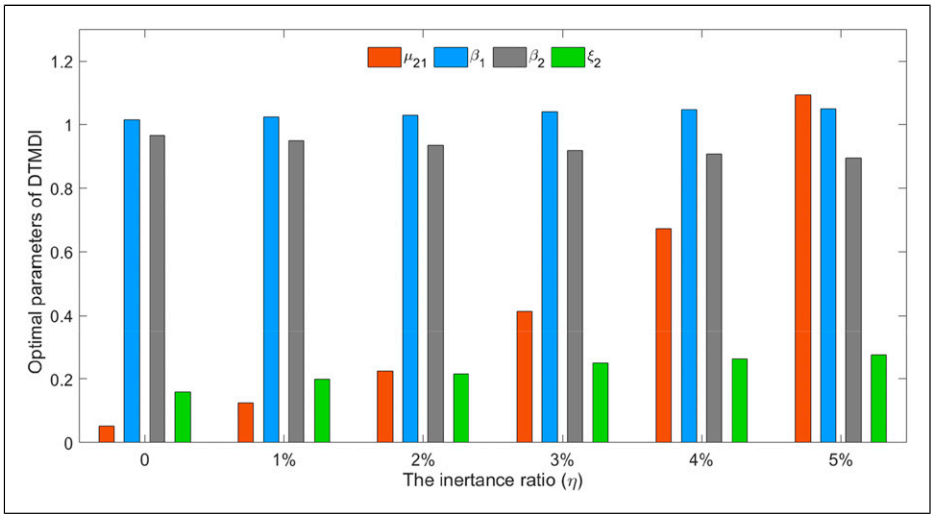

Figure 3. Variation of the DTMDI parameters as the inertance ratio changes from 0% to 5%.

$$RMS_X = \sqrt{\frac{\sum_1^n (X_i)^2}{n}}, \tag{16}$$

in which X_i is the sampling value of the structural peak displacement at the excitation frequency ω_i in the frequency range of $[\omega_{lo}, \omega_{up}]$. From that, a dimensionless quantity of $RMS_{\overline{X}}$ is expressed by (Cao, 2023):

$$RMS_{\overline{X}} = \sqrt{\frac{\sum_1^n \left(\overline{X}_i\right)^2}{n}} = \sqrt{\frac{\sum_1^n \left(\frac{X_i}{F_0/K_s}\right)^2}{n}} \tag{17}$$

with $K_s = M_s\omega_s^2$.

Based on the first criterion, the vibration reduction of each vibration absorber is defined as follows:

$$\varphi_{DMF} = \frac{DMF_{max}^{UC} - DMF_{max}^{device}}{DMF_{max}^{UC}} \times 100\% . \tag{18}$$

Based on the second criterion, the vibrating energy reduction for each device is determined by

$$\varphi_{RMS} = RMS\frac{\overline{X}^{UC} - RMS_{\overline{X}}^{device}}{RMS_{\overline{X}}^{UC}} \times 100\% . \tag{19}$$

In the above equations, "UC" represents the uncontrolled structure, while "device" refers to the structure that is equipped with a vibration mitigation device.

4.2. Performance of DTMDI

To assess the vibration reduction effectiveness of an optimized DTMDI, its performance is analyzed and compared against that of the optimal TMDI which has the same weight and inertance ratio as the DTMDI.

As reported in Ref (Cao, 2023), the values of DMF_{max} and $RMS_{\overline{X}}$ of the uncontrolled structure are 50.0 and 8.8, respectively. Based on the data presented in Table 3 and Table 4, the values of DMF_{max}, φ_{DMF}, $RMS_{\overline{X}}$, and φ_{RMS} of configurations of DTMDI and TMDI are determined. Table 5 lists these values of the optimal DTMD and optimal configurations of DTMDI at $\mu = 2\%$. Similarly, Table 6 also reports the values of DMF_{max}, φ_{DMF}, $RMS_{\overline{X}}$, and φ_{RMS}

Table 5. DMF_{max}, φ_{DMF}, $RMS_{\overline{X}}$, and φ_{RMS} of the optimal DTMDI and DTMD at $\mu = 2\%$.

	DTMDI				DTMD			
η	DMF_{max}	φ_{DMF}	$RMS_{\overline{X}}$	φ_{RMS}	DMF_{max}	φ_{DMF}	$RMS_{\overline{X}}$	φ_{RMS}
0%					6.92	86.2%	3.95	55.2%
1%	5.81	88.4%	3.61	59.0%				
2%	5.11	89.8%	3.37	61.7%				
3%	4.64	90.7%	3.20	63.6%				
4%	4.28	91.4%	3.07	65.1%				
5%	4.00	92.0%	2.95	66.5%				

Table 6. DMF_{max}, φ_{DMF}, $RMS_{\overline{X}}$, and φ_{RMS} of the optimal TMDI and TMD at $\mu = 2\%$.

	TMDI				TMD			
η	DMF_{max}	φ_{DMF}	$RMS_{\overline{X}}$	φ_{RMS}	DMF_{max}	φ_{DMF}	$RMS_{\overline{X}}$	φ_{RMS}
0%					8.57	82.9%	4.21	52.2%
1%	7.21	85.6%	3.84	56.4%				
2%	6.37	87.3%	3.60	59.1%				
3%	5.78	88.4%	3.42	61.1%				
4%	5.34	89.3%	3.27	62.8%				
5%	4.99	90.0%	3.15	64.2%				

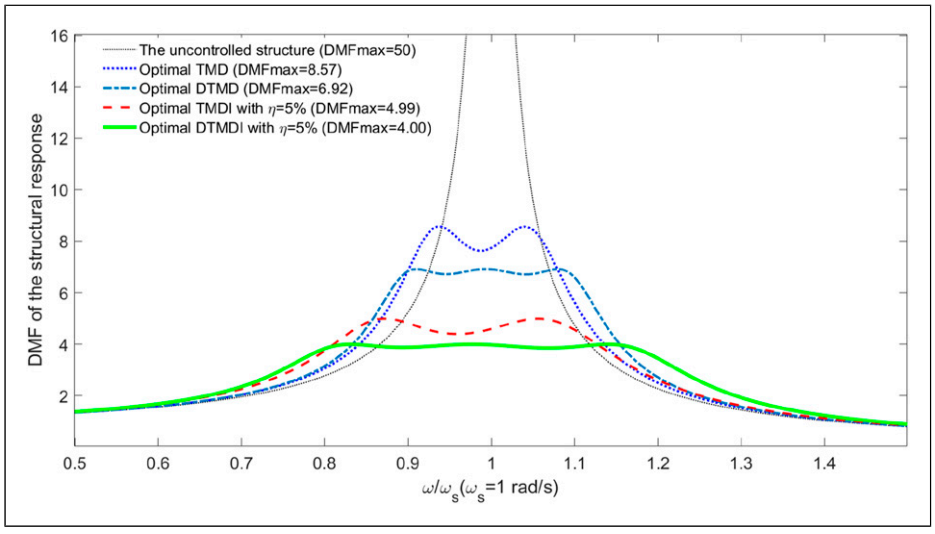

Figure 4. A comparison on frequency response functions of the structure controlled by the optimal TMD, DTMD, TMDI with $\eta = 5\%$, and DTMDI with $\eta = 5\%$ in the case of $\mu = 2\%$.

of the optimal TMD and TMDI configurations in the case of $\mu = 2\%$.

As previously discussed, based on the DMF_{max} value, a configuration of DTMDI/TMDI that yields a lower DMF_{max} value is regarded as more efficient. This is also applied to the second criterion when assessing the performance of DTMDI/TMDI according to the $RMS_{\overline{X}}$ value. From the data reported in Table 5 regarding to the optimal configurations of DTMD/DTMDI, it can be seen that, when adding the grounded inerter to the DTMD, the control performance of DTMD is significantly enhanced. This performance improvement increases from 2.2% to 5.8% for φ_{DMF} and from 3.8% to 11.3% for φ_{RMF} when the inertance ratio rises from 1% to 5%. Similarly, this is also

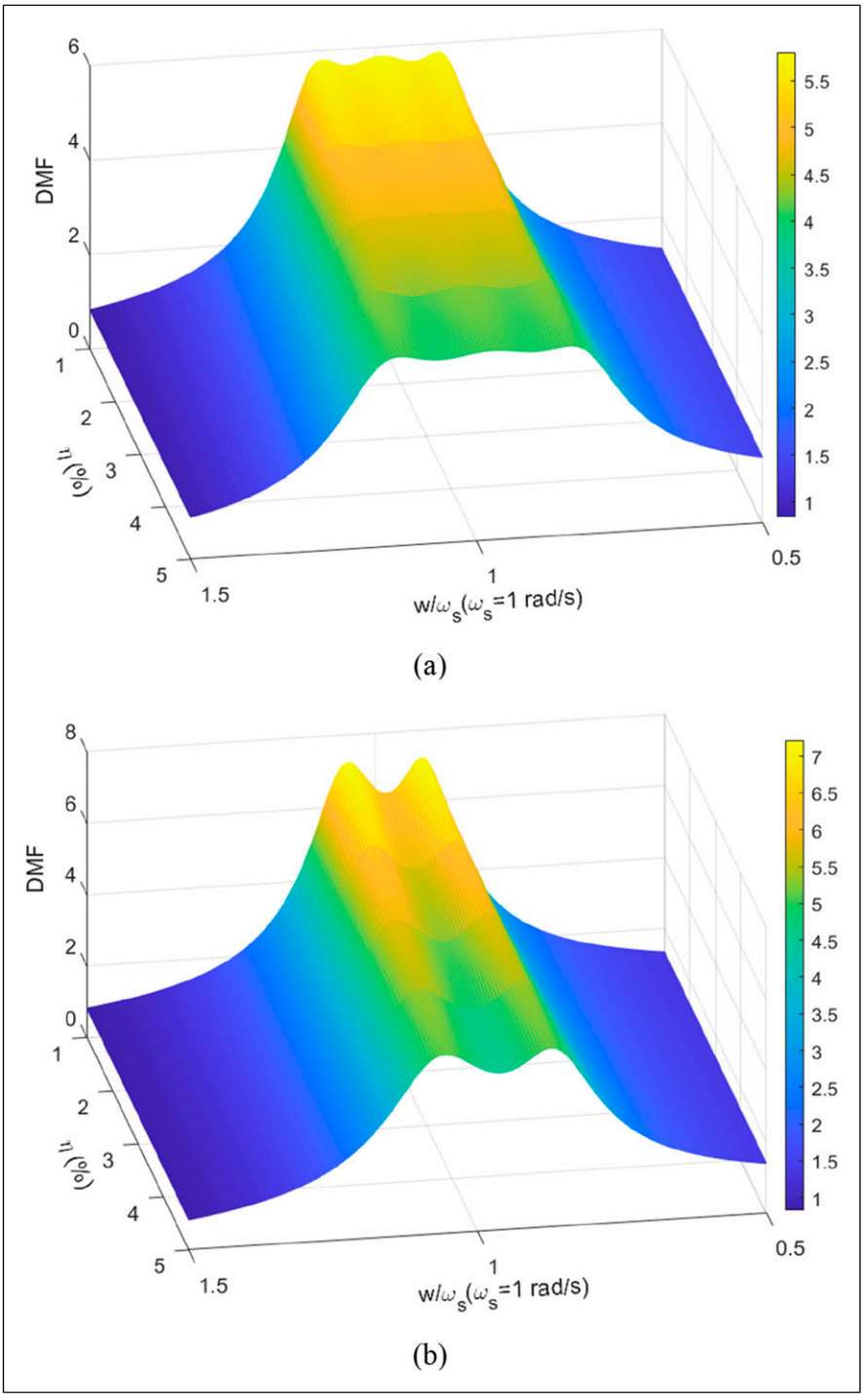

Figure 5. DMF surface of the structure controlled by (a) the DTMDI and (b) the TMDI when the inertance ratio changes from 1% to 5% at $\mu = 2\%$.

true for the optimal TMD and configurations of TMDI. By using an inerter with the inertance ratio within [1%, 5%] to connect the TMD to the ground, the improvement in the effectiveness of TMD lifts from 2.7% to 7.1% and from 4.2% to 12.0% on the φ_{DMF} and φ_{RMF} indicators, respectively.

Based on the same weight and inertance ratio, it is evident that the control effectiveness of optimized configurations of DTMDI is higher than those of TMDI. In particular, the structural vibration reduction achieved from the optimal DTMDI with $\mu = 2\%$ and $\eta = 2\%$ is 89.8%, while this value of the optimal TMDI (at $\mu = 2\%$ and

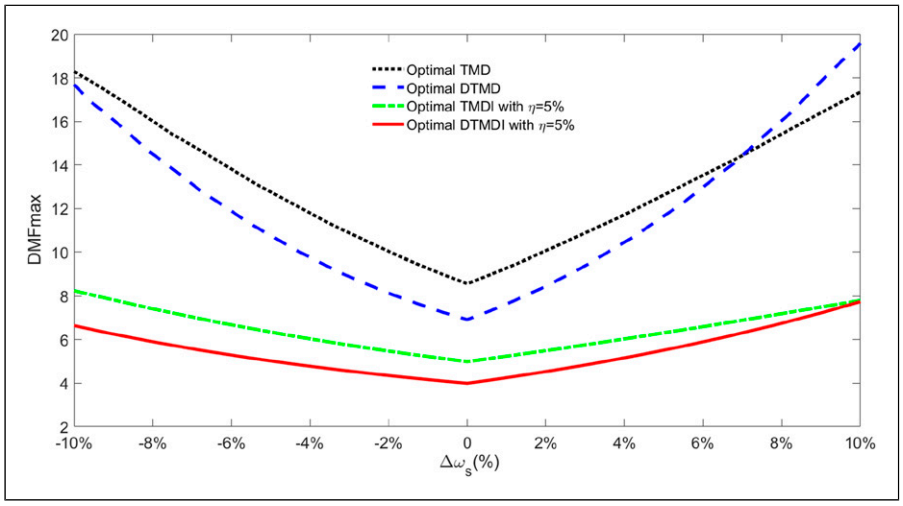

Figure 6. Effect of changes in the structural natural frequency on the effectiveness of the optimal TMD, DTMD, TMDI, and DTMDI at $\mu = 2\%$.

$\eta = 2\%$) is 87.3%. In another comparison, the vibration reduction capacity of the optimal DTMDI with $\mu = 2\%$ and $\eta = 2\%$ is similar to that of TMDI at $\mu = 2\%$ and $\eta = 5\%$ (89.8% compared with 90.0%).

For optimized configurations of DTMDI/TMDI, the optimal DTMDI/TMDI configuration with a larger inertance ratio is more effective. This can be explained by the fact that when the inertance ratio (η) increases, the total mass ratio of DTMDI/TMDI (consisting of the real mass μ and the apparent mass η) rises. This leads to an increase in the control performance of DTMDI/TMDI. An important aspect is that as η increases, the damping coefficient of the TMDI/DTMDI also increases (as reported in Table 3 and Table 4). Furthermore, with the same value of η, the optimal DTMDI configuration requires a larger damping coefficient compared to that of the TMDI configuration. For example, at $\mu = 2\%$ and $\eta = 3\%$, the damping coefficient of the optimal DTMDI is 0.249 (see Table 3), while the ξ value of the optimized TMDI is 0.215 (see Table 4).

Figure 4 shows a comparison on the frequency response functions of the main structure equipped with various devices: the optimal TMD, TMDI, DTMD and DTMDI, in which the optimal configurations for TMDI and DTMDI are based on the inertance ratio of $\eta = 5\%$. From this figure, it is evident that the peak dynamic magnification factor of the structural response significantly decreases when using the optimal TMDI or DTMDI configurations. Notably, the DTMDI configuration produces a DMF_{max} value of 4.00, which is lower than the DMF_{max} value of 4.99 obtained with the TMDI configuration. It can be concluded that the DTMDI provides a higher control performance over a broader excitation frequency domain compared with the TMDI in suppressing structural vibration.

With the mass ratio of $\mu = 2\%$, Figure 5 depicts DMF response surfaces of the primary structure controlled by the DTMDI and the TMDI as the inertance ratio varies from 1% to 5%. As shown in Figure 5, the DMF response surface of the structure with the DTMDI exhibits a three-peak characteristic, and its peak region remains relatively flat over a broader range of excitation frequencies (refer to Figure 5(a)). In contrast, the response surface of the structure with the TMDI displays a two-peak characteristic, with a peak region that is not flat over a narrower frequency range (refer to Figure 5(b)).

4.3. Robustness of DTMDI

In practice, the stiffness and mass of the primary structure may be different from the initial calculated values due to errors in measurement progress (Yamaguchi and Harnpornchai, 1993), equipment replacement on the structure (Cao and Tran, 2023), or even environmental factors (e.g., snow accumulation). This leads to the natural frequency of the structure which differs from the initial calculated value (as reported in Table 1). Thus, the DTMDI can be detuned. This is why a survey on the robustness of the DTMDI against changes in the structural natural frequency (ω_s) is necessary.

It is assumed that the change in the structural natural frequency, $\Delta\omega_s(\%)$, ranges from -10% to 10%. Figure 6 shows the robustness of the optimal TMD, DTMD, TMDI, and DTMDI against variations in the structural frequency within the range of [-10%, 10%] with the mass ratio $\mu = 2\%$. Here, the configurations of TMDI and DTMDI are optimized for the inertance ratio $\eta = 5\%$. In Figure 6, the optimal devices (including TMD, DTMD, TMDI, and DTMDI) have the highest control effectiveness at the nominal natural frequency ($\Delta\omega_s = 0\%$). As shown in Table 5 and Table 6, the DMF_{max} value of the structural response with the optimal TMD, DTMD, TMDI, and DTMDI at $\Delta\omega_s = 0\%$ are 8.57, 6.92, 4.99, and 4.0, respectively. However, when the natural frequency of the primary structure changes, the optimized

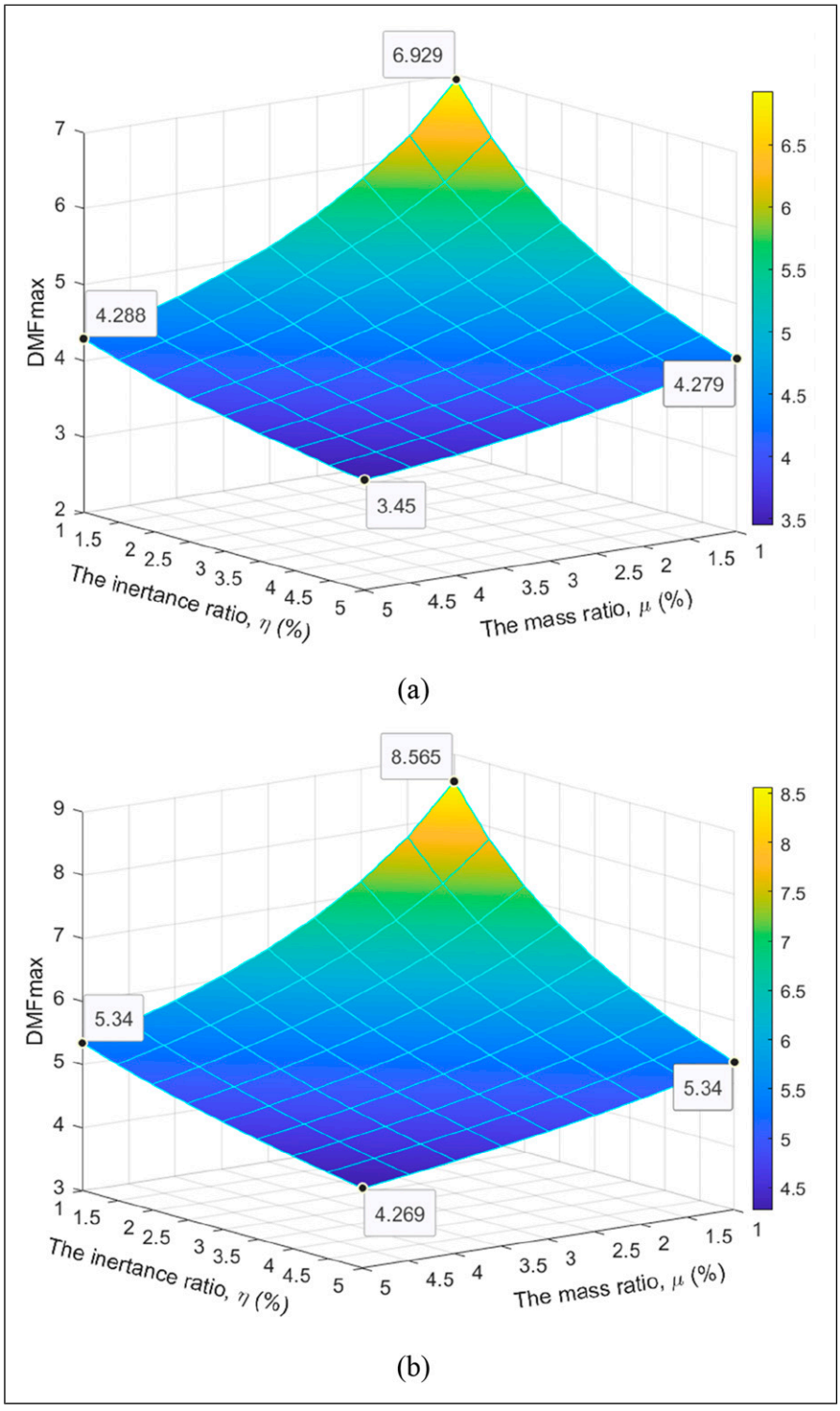

Figure 7. Effects of the inertance ratio and mass ratio on the structure response as μ and η change from 1% to 5%: (a) for DTMDI and (b) for TMDI.

TMD, DTMD, TMDI, and DTMDI become non-optimized vibration absorbers, and they are less effective. The results presented in the figure indicate that the optimal DTMDI configuration is significantly more robust than the DTMD. Additionally, it also demonstrates greater robustness compared to the TMD. Nevertheless, when the structural natural frequency increases, the DTMDI becomes less robust than the TMDI.

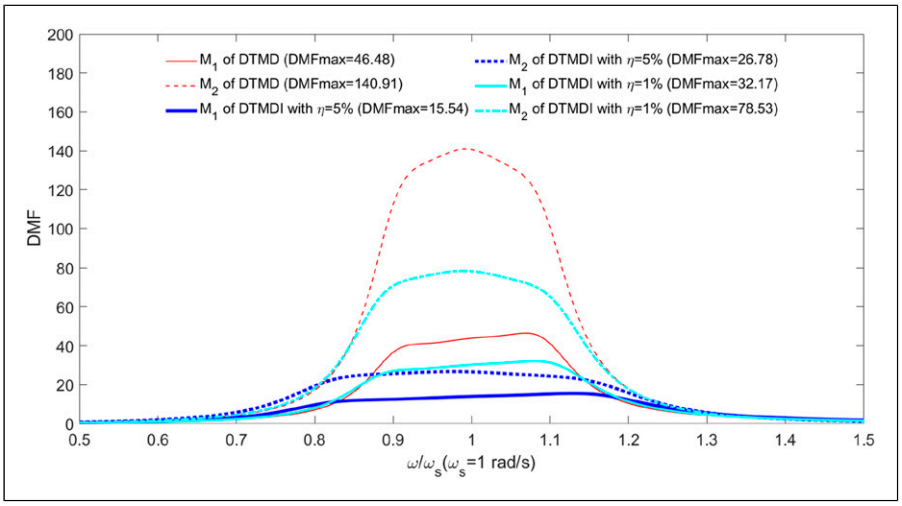

Figure 8. DMF curves of the TMD1 and TMD2 masses of the optimal DTMDIs (with η = 1% and 5%) and DTMD at $\mu = 2\%$.

4.4. Effects of the inertance ratio and mass ratio on the structural response

This section investigates the effects of the inertance ratio (η) and the mass ratio (μ) on the structural response. When both the inertance and mass ratios vary within the same range of [1%, 5%], Figures 7(a) and 7(b) depict the DMF_{max} response surface of the structure controlled by the DTMDI and TMDI, respectively. As observed in Figure 7(a), the DMF_{max} value of the structural response reduces from 6.929 (corresponding to the optimal DTMDI configuration with $\eta = \mu = 1\%$) to 3.45 (with the DTMDI configuration at $\eta = \mu = 5\%$). Meanwhile, the DMF_{max} value of the structural response with the optimized TMDI configurations drops from 8.565 (for the TMDI configuration with $\eta = \mu = 1\%$) to 4.269 (with the optimized TMDI configuration at $\eta = \mu = 5\%$) (refer to Figure 7(b)). It is clear that a DTMDI optimized is significantly more effective than a TMDI. For instance, the control performance of the optimal DTMDI configuration with $\mu = 1\%$ and $\eta = 5\%$ (DMF_{max} = 4.279) is comparable to that of the optimal TMDI configuration with $\mu = 5\%$ and $\eta = 5\%$ (DMF_{max} = 4.269), demonstrating a significant reduction in the device's weight added to the primary structure.

On the other hand, these DMF_{max} surfaces represent the Pareto optimization surfaces for both DTMDI and TMDI, addressing three primary objectives: the additional weight of the device on the main structure, the inertance required of the grounded inerter, and the vibration suppression performance. This provides engineers with a framework to balance design objectives related to the mass, inertance, and effectiveness of each absorber used.

4.5. Vibrations of masses M_1 and M_2 in DTMDI

To further understand how masses M_1 and M_2 in the optimal DTMDI oscillates, Figure 8 shows the DMF curves of the TMD1 and TMD2 masses of the optimal DTMDIs and DTMD in the case of μ = 2%, in which the inertance ratios of the optimal DTMDIs are η = 1% and 5%. As observed from Figure 8, with a given inertance ratio of DTMDI, the maximum DMF values of the mass M_1 in the DTMDIs are much smaller than that of M_1 in the DTMD. Particularly, the DMF_{max} values of the mass M_1 in the DTMDs with η = 1% and 5% are 32.17 and 15.54, respectively, while the maximum vibration of M_1 in the DTMD is at DMF_{max} = 46.48. This is also true for vibrations of M_2 in the DTMDIs and in the DTMD. It is possible to conclude that the inerter plays a core role in reducing significantly the stroke of M_1 and M_2 in the DTMDI compared with their vibrations in the DTMD. Moreover, a larger inertance ratio results in greater oscillation reduction for the TMD1 and TMD2 masses.

5. Conclusions

The DTMD has been demonstrated to be more efficient than a traditional TMD (Cao and Tran, 2023). To further improve the performance and robustness of DTMD, an upgraded version of DTMD for structural vibration control was proposed in this research. In the innovative type of DTMD, the DTMD was linked to the ground through a linear inerter. Modeling of the system consisting of a SDOF structure with a DTMDI was established. The optimal configurations of the DTMDI corresponding to various inertance ratios were then found using the BCMO algorithm. Studies on the effects of changes in the structural properties as well as the mass and inertance of DTMDI to the control effectiveness and robustness of DTMDI were conducted. The outstanding findings obtained from this work include:

(a) An optimal DTMDI is significantly more effective and robust than an optimal DTMD with the same weight as the DTMDI, in which the optimal configuration of

DTMDI with a higher inertance ratio produces higher effectiveness.

(b) With the same mass and inertance, the DTMDI yields higher performance compared to the TMDI. Thus, using a DTMDI instead of a TMDI offers a significant reduction in the weight of the device on the main structure.

(c) The DTMDI is more robust than both the DTMD and TMD against the variation of the structure's natural frequency, but the DTMDI becomes less robust than the TMDI when the structural frequency increases.

(d) Three-objective optimization surfaces for both DTMDI and TMDI generated in this work provide engineers with a frame to balance design objectives related to the mass, inertance, and performance of each device employed.

(e) With a given inertance ratio, vibrations of M_1 and M_2 in the DTMDI are significantly smaller than those of M_1 and M_2 in the DTMD. Furthermore, the larger the inertance ratio, the greater the oscillation reduction of the TMD1 and TMD2 masses.

The inerter of the DTMDI connected to the ground may be a disadvantage of DTMDI for seismic protection of structures. However, the practical applicability of the proposed damper in civil structures under the other types of loads is very significant. For example, DTMDI can be equipped on offshore platforms to reduce structural responses induced by wave and wind loadings, or it can be integrated into bridges to mitigate vertical vibrations caused by pedestrian and vehicle loads. In addition, DTMDI can be used for base-isolated structures, as mentioned in the previous studies (De Angelis et al., 2019; De Domenico and Ricciardi, 2018).

Although the findings discussed in this work were based on harmonic excitation forces, the proposed device is expected to perform well under random excitations. In future studies, the effectiveness of the DTMDI in controlling the dynamic response of various types of structures subjected to random excitations will be investigated.

Declaration of conflicting interests

The author(s) declared no potential conflicts of interest with respect to the research, authorship, and/or publication of this article.

Funding

The author(s) received no financial support for the research, authorship, and/or publication of this article.

ORCID iD

Huong Quoc Cao https://orcid.org/0000-0002-6352-3787

Data availability statement

All data that support the findings of this study are included within the article.

References

Araz O (2021a) Optimization of three-element tuned mass damper for single degree of freedom structures under ground acceleration. *El-Cezeri Journal of Science and Engineering* 8(3): 1264–1271.

Araz O (2021b) Optimum passive tuned mass damper systems for main structures under harmonic excitation. *Mühendislik Bilimleri ve Tasarım Dergisi* 9(4): 1062–1071.

Araz O (2024) Effect of PGV/PGA ratio on seismic-induced vibrations of structures equipped with parallel tuned mass dampers considering SSI. *Structures* 68: 107188.

Araz O and Elias S (2024) Performance of differently arranged double-tuned mass dampers for structural seismic response control including soil-structure interaction. *Engineering Structures* 319: 118841.

Araz O and Kahya V (2021) Optimization of non-traditional tuned mass damper for damped structures under harmonic excitation. *Uludağ University Journal of The Faculty of Engineering* 26(3): 1021–1034.

Baduidana M and Kenfack-Jiotsa A (2024) Parameters optimization of three-element dynamic vibration absorber with inerter and grounded stiffness. *Journal of Vibration and Control* 30(7-8): 1548–1565.

Balendra T, Wang CM and Cheong HF (1995) Effectiveness of tuned liquid column dampers for vibration control of towers. *Engineering Structures* 17(9): 668–675.

Bui H-L, Tran N-A and Cao HQ (2023a) Active control based on hedge-algebras theory of seismic-excited buildings with upgraded tuned liquid column damper. *Journal of Engineering Mechanics* 149(1): 04022091.

Cao HQ (2023) Combined tuned mass dampers for structural vibration control. *International Journal of Non-linear Mechanics*.

Cao HQ and Tran N-A (2023) Multi-objective optimal design of double tuned mass dampers for structural vibration control. *Archive of Applied Mechanics* 93(5): 2129-2144.

Cao HQ, Tran N-A and Nguyen X-T (2024b) Tuned two-mass dampers for vibration control of offshore platforms. *Engineering Research Express* 6(3): 35511.

Chang CC (1999) Mass dampers and their optimal designs for building vibration control. *Engineering Structures* 21(5): 454–463.

Chang CC and Hsu CT (1998) Control performance of liquid column vibration absorbers. *Engineering Structures* 20(7): 580–586.

De Angelis M, Giaralis A, Petrini F, et al. (2019) Optimal tuning and assessment of inertial dampers with grounded inerter for vibration control of seismically excited base-isolated systems. *Engineering Structures* 196: 109250.

De Domenico D and Ricciardi G (2018) An enhanced base isolation system equipped with optimal tuned mass damper inerter (TMDI). *Earthquake Engineering & Structural Dynamics* 47(5): 1169–1192.

Den Hartog JP (1985) *Mechanical Vibrations*. New York: Dover Publications, Inc.

Di Matteo A, Masnata C, Adam C, et al. (2022) Optimal design of tuned liquid column damper inerter for vibration control. *Mechanical Systems and Signal Processing* 167: 108553.

Diana G, Resta F, Sabato D, et al. (2013) Development of a methodology for damping of tall buildings motion using TLCD devices. *Wind and Structures* 17(6): 629–646.

Etedali S and Rakhshani H (2018) Optimum design of tuned mass dampers using multi-objective cuckoo search for buildings under seismic excitations. *Alexandria Engineering Journal* 57(4): 3205–3218.

Gao H, Kwok KSC and Samali B (1999) Characteristics of multiple tuned liquid column dampers in suppressing structural vibration. *Engineering Structures* 21(4): 316–331.

Giaralis A and Petrini F (2017) Wind-induced vibration mitigation in tall buildings using the tuned mass-damper-inerter. *Journal of Structural Engineering* 143(9): 04017127.

Gil-Martín LM, Carbonell-Márquez JF, Hernández-Montes E, et al. (2012) Dynamic magnification factors of SDOF oscillators under harmonic loading. *Applied Mathematics Letters* 25(1): 38–42.

Hui Y, Yang Z, Xia C, et al. (2024) Study on vibration control performance of pendulum TMD with additional stoppers and its application on high-rise buildings. *Journal of Wind Engineering and Industrial Aerodynamics* 254: 105926.

Kahya V and Araz O (2019) A sequential approach based design of multiple tuned mass dampers under harmonic excitation. *Journal Engineering and Natural Sciences* 37(1): 225–239.

Kendo-Nouja B, Baduidana M, Kenfack-Jiotsa A, et al. (2024) Vibration reduction of primary structure using optimum grounded inerter-based dynamic vibration absorber. *Archive of Applied Mechanics* 94(1): 137-156.

Konar T and Ghosh A (2024) Tuned mass damper inerter for seismic control of multi-story buildings: ten years since inception. *Structures* 63: 106459.

Le-Duc T, Nguyen Q-H and Nguyen-Xuan H (2020) Balancing composite motion optimization. *Information Sciences* 520: 250–270.

Ma R, Bi K and Hao H (2021) Inerter-based structural vibration control: a state-of-the-art review. *Engineering Structures* 243: 112655.

Marian L and Giaralis A (2014) Optimal design of a novel tuned mass-damper–inerter (TMDI) passive vibration control configuration for stochastically support-excited structural systems. *Probabilistic Engineering Mechanics* 38: 156–164.

McCall J (2005) Genetic algorithms for modelling and optimisation. *Journal of Computational and Applied Mathematics* 184(1): 205–222.

Momtaz AA, Abdollahian MA and Farshidianfar A (2017) Study of wind-induced vibrations in tall buildings with tuned mass dampers taking into account vortices effects. *International Journal of ineering* 9(4): 385–395.

Pandey DK and Mishra SK (2021) Inerter assisted robustness of compliant liquid column damper. *Structural Control and Health Monitoring* 28(8).

Pisal AY and Jangid RS (2016) Vibration control of bridge subjected to multi-axle vehicle using multiple tuned mass friction dampers. *International Journal of Advanced Structural Engineering (IJASE)* 8(2): 213–227.

Prakash S and Jangid RS (2022) Optimum parameters of tuned mass damper-inerter for damped structure under seismic excitation. *International Journal of Dynamics and Control* 10(5): 1322–1336.

Samali B, Mayol E, Kwok KCS, et al. (2004) Vibration control of the wind-excited 76-story benchmark building by liquid column vibration absorbers. *Journal of Engineering Mechanics* 130(4): 478–485.

Shah MU and Usman M (2022) An experimental study of tuned liquid column damper controlled multi-degree of freedom structure subject to harmonic and seismic excitations. *PLoS One* 17(6): e0269910.

Smith MC (2002) Synthesis of mechanical networks: the inerter. *IEEE Transactions on Automatic Control* 47(10): 1648–1662.

Tran N-A, Bui H-L and Cao Q-H (2024) U-shaped and V-shaped tuned liquid column dampers in vibration reduction of earthquake-induced buildings: a comparative study. *Structures* 65: 106669.

Tran N-A, Hoang V-B, Bui H-L, et al. (2025) Upgraded double tuned mass dampers for vibration control of structures under earthquakes. *Computers & Structures* 310: 107700.

Varadarajan N and Nagarajaiah S (2004) Wind response control of building with variable stiffness tuned mass damper using empirical mode decomposition/hilbert transform. *Journal of Engineering Mechanics* 130(4): 451–458.

Vellar LS, Ontiveros-Pérez SP, Miguel LFF, et al. (2019) Robust optimum design of multiple tuned mass dampers for vibration control in buildings subjected to seismic excitation. *Shock and Vibration* 2019: 1–9.

Wang Q, Tiwari ND, Qiao H, et al. (2020) Inerter-based tuned liquid column damper for seismic vibration control of a single-degree-of-freedom structure. *International Journal of Mechanical Sciences* 184: 105840.

Wang L, Shi W and Zhou Y (2022) Adaptive-passive tuned mass damper for structural aseismic protection including soil–structure interaction. *Soil Dynamics and Earthquake Engineering* 158: 107298.

Wang Z, Chai X, Peng S, et al. (2024) A novel tuned liquid mass damper for low-frequency vertical vibration control: model experiments and field tests. *Mechanical Systems and Signal Processing* 220: 111702.

Wu J-C, Shih M-H, Lin Y-Y, et al. (2005) Design guidelines for tuned liquid column damper for structures responding to wind. *Engineering Structures* 27(13): 1893–1905.

Wu Q, Zhao W, Zhu W, et al. (2018) A tuned mass damper with nonlinear magnetic force for vibration suppression with wide frequency range of offshore platform under earthquake loads. *Shock and Vibration* 2018: 1–18.

Yalla SK and Kareem A (2000) Optimum absorber parameters for tuned liquid column dampers. *Journal of Structural Engineering* 126(8): 906–915.

Yamaguchi H and Harnpornchai N (1993) Fundamental characteristics of multiple tuned mass dampers for suppressing harmonically forced oscillations. *Earthquake Engineering & Structural Dynamics* 22(1): 51–62.

Yang JN, Agrawal AK, Samali B, et al. (2004) Benchmark problem for response control of wind-excited tall buildings. *Journal of Engineering Mechanics* 130(4): 437–446.

Zuo L (2009) Effective and robust vibration control using series multiple tuned-mass dampers. *Journal of Vibration and Acoustics* 131(3): 11.

Appendix A

The TMDI-structure system

An analytical model of the system TMDI-structure under an external force excitation is shown in Figure 9. The TMD has the mass M_T, the stiffness K_T and the damping coefficient C_T. The equations of motion of the system are expressed by:

$$(M_T + b)\ddot{X}_s(t) + (M_T + b)\ddot{X}_T(t) + C_T\dot{X}_T(t) + K_T X_T(t) = 0, \tag{A1}$$

$$M_s\ddot{X}_s(t) + C_s\dot{X}_s(t) + K_s X_s(t) - C_T\dot{X}_T(t) - K_T X_T(t) = F(t). \tag{A2}$$

Here, X_s is the structural displacement and X_T is the displacement of the TMD relative to the structure.

The natural frequency of the TMDI is

$$\omega_{T1} = \sqrt{\frac{K_T}{M_T + b}}. \tag{A3}$$

The damping ratio of the TMD is

$$\xi_{T1} = \frac{C_T}{2M_T\omega_T}. \tag{A4}$$

The mass ratio between the TMD and structure is

$$\mu_T = \frac{M_T}{M_s}. \tag{A5}$$

The total mass ratio between the TMDI and the structure is given by

$$\overline{\mu} = \mu_T + \eta \tag{A6}$$

with the inertance ratio of η.

The tuning ratio of the TMDI is

$$\beta_{T1} = \frac{\omega_T}{\omega_s}. \tag{A7}$$

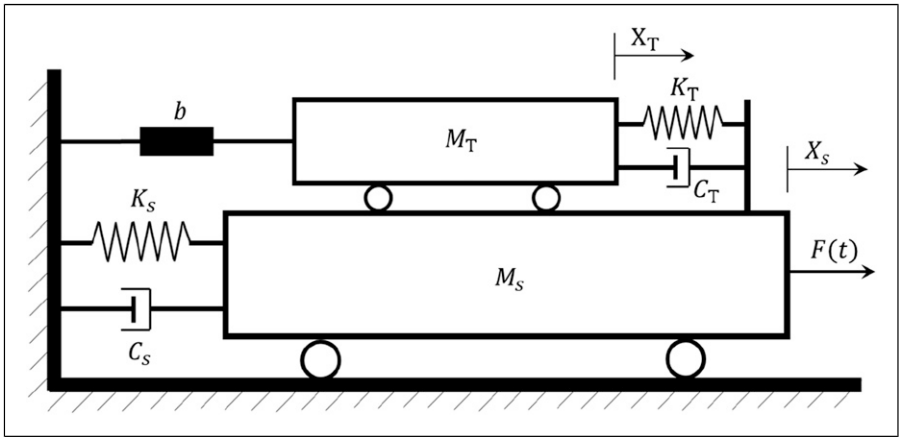

Figure 9. Analytical model of the TMDI-structure system.